# Equilibria for the relative motion of three heavy spheres in Stokes fluid flow

Maria L. Ekiel-Jeżewska* and Eligiusz Wajnryb
*Institute of Fundamental Technological Research, Polish Academy of Sciences, Świętokrzyska 21, 00-049 Warsaw, Poland*
(Received 23 August 2005; revised manuscript received 30 January 2006; published 26 April 2006)

Dynamics of three identical solid spheres falling under gravity in low-Reynolds-number fluid flow is investigated. Stationary solutions are found. Their stability is discussed. Phase portraits for two types of symmetric motions are calculated.

DOI: 10.1103/PhysRevE.73.046309 PACS number(s): 47.20.−k, 82.70.−y

## I. INTRODUCTION

The mechanism of clustering of micro-objects moving in water, as well as motility and shape of the clusters, attract a lot of interest in various biological and industrial contexts. In these problems, it is important to understand interactions between the micro-objects [e.g., bacteria [1] or microelectromechanial systems) caused by the fluid flow, and especially to determine stationary and periodic trajectories. In a quiescent viscous infinite fluid, two identical spheres always settle under gravity with no change of relative configuration. Therefore the simplest interesting model system is a cluster, which consists of three identical heavy spheres. Its dynamics is nonlinear, and in general chaotic, as shown numerically within the point-force approximation [2]. Symmetric periodic motions of three point particles and of three spheres located at vertices of an isosceles triangle exist [3–5] and the equilateral horizontal triangle is the stationary stable solution.

In this work, other stationary solutions are found and their properties are discussed, extending the ideas from Ref. [6]. We start from analyzing such equilibria, where the particle centers form an isosceles vertical triangle with the horizontal base (in the following, such a configuration will be called "symmetrical"), and at least two spheres touch each other. In Sec. III, the system of equations describing the motion of the symmetrical configurations is specified, and the method to solve it is outlined. In Sec. IV, the symmetrical equilibrium configurations of the spheres are determined. In Sec. V, the sphere centers are aligned horizontally, their motion is evaluated and compared with the point-particle approximation. It is shown that the spheres tend to an equilibrium configuration. In Sec. VI, the asymptotic dynamics of the symmetrical configurations close to this equilibrium is explicitly solved and the equilibrium is shown to be stable against all the symmetrical perturbations. In Sec. VII, the phase portrait of the relative symmetrical motion of the spheres is determined. In Sec. VIII, the symmetrically stable equilibrium is shown to be unstable against nonsymmetrical perturbations. To show physical significance of this equilibrium, another illustrative exemplary dynamics is investigated: isosceles triangles with a horizontal base and a single pair of touching spheres. The conclusions are given in Sec. IX.

*Electronic address: mekiel@ippt.gov.pl

## II. MOBILITY PROBLEM

An infinite fluid of viscosity $\eta$ is considered. Its low-Reynolds-number flow is generated by settling of three identical spheres under gravity $\mathbf{F}=-F\hat{\mathbf{e}}_z$, with instantaneous velocities of the order of the Stokes velocity [the Strouhal number is $\mathcal{O}(1)$]. The fluid velocity $\mathbf{v}(\mathbf{r})$ and pressure $p(\mathbf{r})$ satisfy the stationary Stokes equations [7]

$$\eta\nabla^2\mathbf{v}-\nabla p=\mathbf{0},\quad \nabla\cdot\mathbf{v}=0. \tag{1}$$

The stick boundary conditions are assumed at the surfaces of the spheres. Positions of the sphere centers $\boldsymbol{r}_i(t)$ satisfy the following equations:

$$\dot{\boldsymbol{r}}_i(t)=\left[\sum_{k=1}^{3}\boldsymbol{\mu}_{ik}\right]\cdot\boldsymbol{F},\quad i=1,2,3. \tag{2}$$

The $3\times3$ mobility matrices $\boldsymbol{\mu}_{ik}$ depend on the instantaneous relative configuration of all the spheres, and are evaluated numerically by the multipole expansion [8,9]. The algorithm from Ref. [10] and its accurate numerical FORTRAN implementation described in Ref. [11] are applied, with the multipole order $L=4$. Typically, such a truncation leads to $10^{-4}$ relative error of the friction and mobility coefficients, see, e.g., Tables II and III in Ref. [10]. The set of the ordinary differential equations (2) is solved numerically by the adaptive fourth-order Runge-Kutta method [12]. In the following, distances will be normalized by the sphere diameter $d$, time by $\tau_s=3\pi\eta d^2/F$ (two Stokes times), and mobilities by $1/(3\pi\eta d)$, keeping the same notation. The dimensionless variables satisfy Eq. (2) with $F=1$.

In the point-force approximation, the same units are used, and a single point moves with the Stokes velocity of the single sphere. The point-particle dynamics reads

$$\dot{\boldsymbol{r}}_i=-\sum_{k\neq i}\mathbf{T}_{ik}\cdot\hat{\mathbf{e}}_z-\hat{\mathbf{e}}_z, \tag{3}$$

with the dimensionless Oseen tensor

$$\mathbf{T}_{ik}=\frac{3}{8r_{ik}}(\mathbf{I}+\hat{\boldsymbol{r}}_{ik}\hat{\boldsymbol{r}}_{ik}), \tag{4}$$

the unit vectors $\hat{\boldsymbol{r}}_{ik}=\hat{\boldsymbol{r}}_{ik}/r_{ik}$ and the unit tensor $\mathbf{I}$. Equation (3) is integrated numerically by the adaptive fourth-order Runge-Kutta method [12].

 

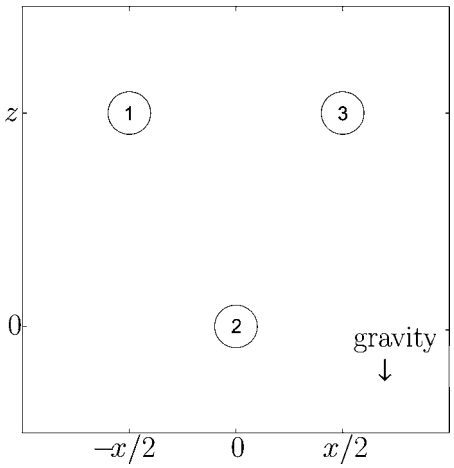


FIG. 1. "Symmetrical" configuration of spheres.

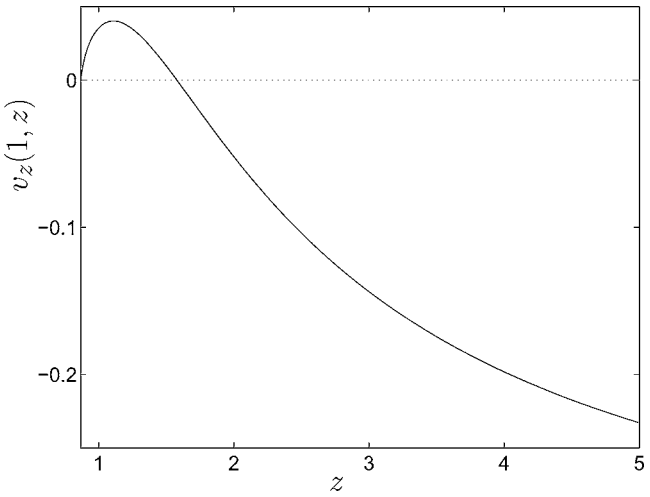


FIG. 2. Mobility function for the symmetrical motion of the touching spheres 1 and 3 with respect to the single sphere 2.

## III. DYNAMICS OF SYMMETRICAL CONFIGURATIONS

Assume for simplicity that initially the sphere centers form an isosceles vertical triangle with the horizontal base. From the symmetry of the Stokes equations it follows that the triangle retains these properties in the course of time. The apex sphere is labeled 2 and the two other spheres are labeled 1 and 3, as indicated in Fig. 1.

Dynamics of particles at vertices of an isosceles vertical triangle with the horizontal base is interesting because of two reasons. First, it might be helpful to understand relative dynamics of three point particles in vertical plane, which in general is chaotic [2]. Second, such a symmetric configuration is related to the family of stable periodic motions as a limiting case. Oscillating particles stay at vertices of an isosceles triangle with the horizontal base; the triangle may come very close (but never exactly) to the vertical position [3–5].

The relative positions are parameterized as

$$\boldsymbol{r}_{12} = (-x/2, 0, z), \tag{5}$$

$$\boldsymbol{r}_{32} = (x/2, 0, z), \tag{6}$$

with $\boldsymbol{r}_{ij} \equiv \boldsymbol{r}_i - \boldsymbol{r}_j$. The distance $x$ between the twin spheres 1 and 3 and the vertical separation $z$ between the twins and the apex sphere 2 satisfy the following system of equations:

$$\dot{x} = v_x(x,z), \tag{7}$$

$$\dot{z} = v_z(x,z), \tag{8}$$

with the initial values $x(0)=x_0$, $z(0)=z_0$. Here $v_x = 2\Sigma_{k=1}^{3}[\mu_{2k,xz} - \mu_{3k,xz}]$, and $v_z = \Sigma_{k=1}^{3}[\mu_{2k,zz} - \mu_{3k,zz}]$, with the Cartesian components of $\boldsymbol{\mu}_{ik}$ dependent only on $x$ and $z$. Once $x(t)$, $z(t)$ are evaluated, then $\mathbf{r}_2 = [0, 0, z_2(t)]$ is obtained by a direct integration of Eq. (2).

## IV. SYMMETRICAL EQUILIBRIA

In this section, equilibria for the dynamics of spheres (7) and (8) will be found. From the symmetry it follows that they are also stationary solutions of the general dynamics (2). The right-hand side of Eq. (7) vanishes if the twin spheres 1 and 3 touch each other and the distance between their centers $x=1$. In this case, the lubrication forces [13] prevent spheres 1 and 3 from a relative motion and $v_x(1,z)=0$ at each point $z$. Equilibrium points $\tilde{z}$ are solutions of the equation $v_z(1,\tilde{z})=0$. The function $v_z(1,z)$ is evaluated numerically and plotted in Fig. 2, for all the configurations with the single sphere 2 below the touching doublet. In this case, $z \geqslant \sqrt{3}/2$, because the spheres do not overlap.

Two equilibria are seen. The first one, with $(x,z)=(1,\sqrt{3}/2)$, corresponds to the touching triplet of spheres, with relative motions excluded by the lubrication forces [13]. It is interesting to see that there exists also another positive root $z_{\mathrm{eq}}$ of the equation $v_z(1,z)=0$. For a given multipole order $1 \leqslant L \leqslant 30$, $z_{\mathrm{eq}}$ is evaluated numerically by the standard bisection method [12]. Next, the limit $L \to \infty$ is taken,

$$z_{\mathrm{eq}} = 1.578634. \tag{9}$$

(The dependence of $z_{\mathrm{eq}}$ on $L$ is discussed in Appendix A.)

In the following, it will be shown that Eq. (9) determines the only equilibrium which attracts all close symmetrical trajectories (5) and (6). Now, vertical relative motion of the horizontal touching doublet located above the singlet will be analyzed, using the function plotted in Fig. 2. In the limit of infinite $z$, the faster doublet and the slower singlet are not influenced by each other and as a result $v_z=-0.3799554$, see, e.g., Ref. [14]. Starting from any $z_0 > z_{\mathrm{eq}}$, the relative distance $z$ between the doublet and the singlet decreases with time, because $v_z<0$. If $z_0 < z_{\mathrm{eq}}$, then $v_z>0$ and $z$ increases with time. It is remarkable that in this case a heavier doublet is repelled by a lighter singlet located below. In both cases, the system tends to the equilibrium position $z_{\mathrm{eq}}$, approaching it after infinite time. Indeed, from Fig. 2 it is clear that $\partial v_z(1,z)/\partial z < 0$, if $z$ is close to $z_{\mathrm{eq}}$, and therefore $|z - z_{\mathrm{eq}}|$ decreases with time exponentially.

Consider now configurations where the touching spheres are below the single one, with $z<0$. The Stokes equations are invariant with respect to the time reversal, superposed

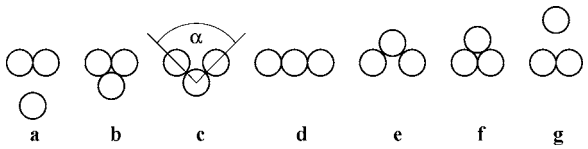


FIG. 3. Equilibrium configurations. a,g: "kissing;" b–f: "chain." Gravity points down.

with the reflection in the horizontal plane, which contains the center of sphere 2. Therefore

$$v_x(x,z) = -v_x(x,-z), \quad v_z(x,z) = v_z(x,-z). \tag{10}$$

In particular, for $z<0$ the relative velocity is immediately obtained from Fig. 2, using the relation $v_z(1,z)=v_z(1,-z)$. Starting from negative $z_0$, trajectories escape from $-z_{\mathrm{eq}}$. If $z_0>-z_{\mathrm{eq}}$, then the doublet is attracted by the singlet and $z\to-\sqrt{3}/2$. If $z_0<-z_{\mathrm{eq}}$, then the doublet is repelled by the singlet and $z\to-\infty$.

Summarizing, equilibria of the dynamics (7) and (8) are located at $(x,z)=(1,\pm 1.578634)$, and on the curve $z^2+x^2/4=1$. In the first case, called "kissing," the only touching spheres are 1 and 3, see Figs. 3(a) and 3(g). In the second case, called "chain," there are at least two pairs of touching spheres: 12 and 23, see Figs. 3(b)–3(f).

The equilibrium configurations settle with a stationary velocity $U$, which is now related to the Stokes velocity $U_s=F/(3\pi\eta d)$. In the first case (kissing), $U/U_s=1.7543000$. In the second case (chain), $1.6304582\leqslant U/U_s\leqslant 1.9022670$; the lower value is obtained if the sphere centers are aligned horizontally [see Fig. 3(d)]; the upper one if they form equilateral triangle [see Figs. 3(b) and 3(f)]. In Fig. 4, the settling velocity $U/U_s$ is depicted as a function of the angle $\alpha$ between the chain links. Configurations reflected in a horizontal plane [e.g., Fig. 3(c)] settle with the same velocity as the original ones [e.g., Fig. 3(e)]. Note that no equilibrium exists within the point-particle approximation.

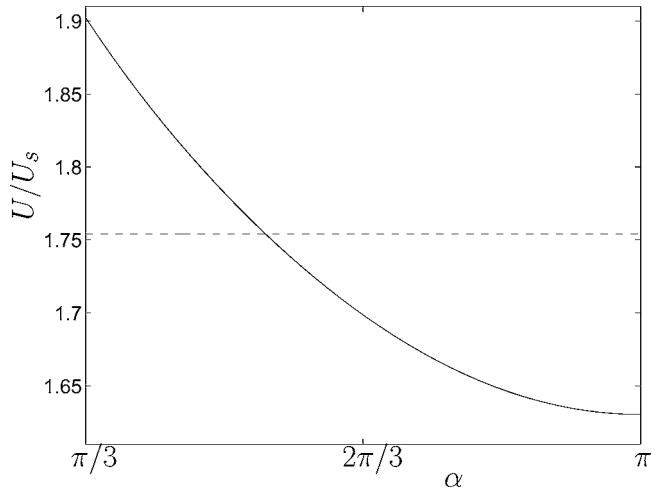


FIG. 4. Settling velocity $U/U_s$ of the "chain" equilibrium configuration versus the angle $\alpha$ between the chain links (solid line). For comparison, the settling velocity of the "kissing" equilibrium configuration is marked (horizontal dashed line).

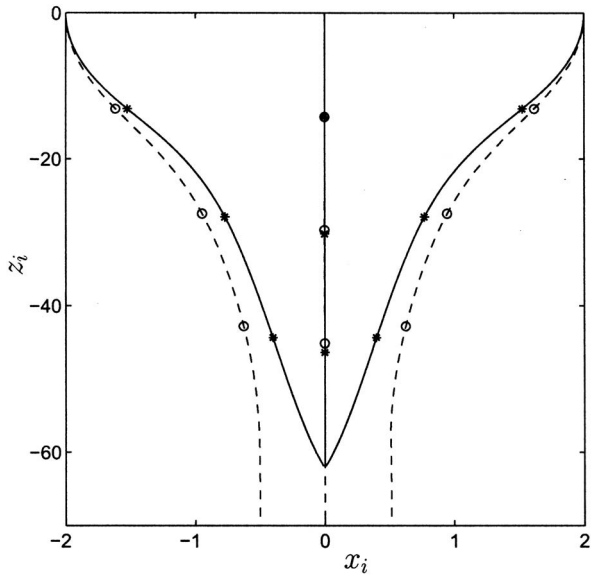


FIG. 5. Trajectories of three sphere centers (dashed lines, circles) and three point particles (solid lines, stars), at $t=0$ centered at $x_1=-2$, $x_2=0$, $x_3=2$, $z_1=z_2=z_3=0$. The symbols represent positions at times $t=10$, 20, and 30.

## V. EVOLUTION OF SPHERES ALIGNED HORIZONTALLY

Now, evolution of nontouching spheres will be studied. In Fig. 5, typical trajectories $z_i(x_i)$ of sphere centers are shown, if they are initially aligned horizontally. The solution of the dynamics (2) is denoted as $\boldsymbol{r}_i(t)=[x_i(t),0,z_i(t)]$, with $i=1,2,3$. Trajectories of point particles, at the beginning coinciding with those of the spheres, after a finite time $t=36.74$ collapse onto a single point, as depicted in Fig. 5, and shown in the companion movie [15].

In the following, the relative two-dimensional dynamics (7) and (8) will be discussed. Evolution of the initial values $x_0$ and $z_0=0$ is of special interest. The distance $\xi=x-1$ between the surfaces of spheres 1 and 3 decreases monotonically, decaying exponentially to zero for long times, as illustrated in Fig. 6.

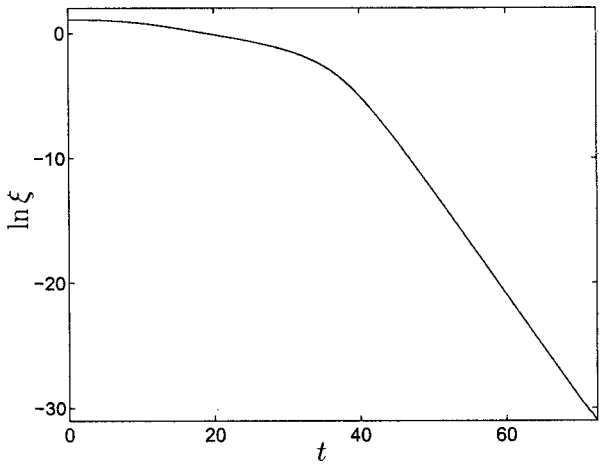


FIG. 6. Size $\xi(t)=x(t)-1$ of the gap between surfaces of the spheres 1 and 3. Initially $\xi_0=3$ and $z_0=0$.

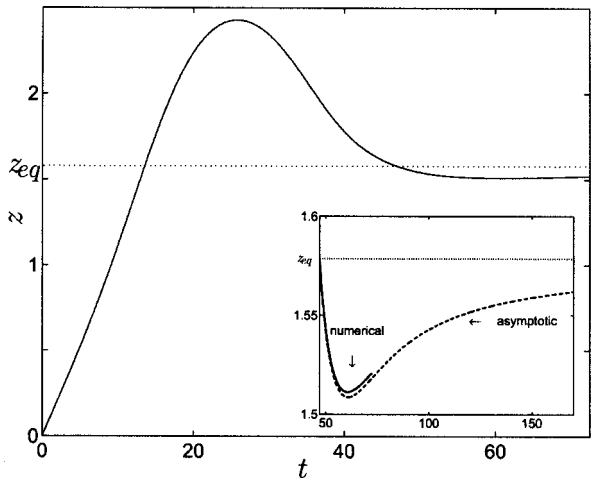


FIG. 7. Vertical separation $z(t)$. Initially $x_0=4$, $z_0=0$. Inset: comparison with the asymptotic expression (16).

For close twin spheres, if $x_0$ is sufficiently small, then their vertical separation $z$ from sphere 2 increases with time. For a large $x_0$, at the beginning $z$ increases, significantly exceeding $z_{\mathrm{eq}}$, then drops down below $z_{\mathrm{eq}}$ to approach it slowly again, as depicted in Fig. 7.

Numerical integration of Eqs. (7) and (8) is limited to the gap sizes $\xi \gtrsim 4\times 10^{-14}$. It is remarkable that for such tiny gaps between the surfaces, the vertical separation $z$ still differs from its equilibrium value $z_{\mathrm{eq}}$ by 3.7%. Physically, this difference is explained by the significant rotation of spheres 1 and 3, with the corresponding dimensionless angular velocities $\Omega_{1y}=3.2\%$, and $\Omega_{3y}=-\Omega_{1y}$. [Angular velocities are normalized by the inverse of the Stokes time, $2U_s/d=2F/(3\pi\eta d^2)$.] This estimation follows from the numerical evaluation of the angular velocity $\Omega_{1y}$ as a function of time, plotted in Fig. 8. ($\Omega_{1y}$ depends linearly on $F$; the proportionality coefficient is easily evaluated by the multipole method if configuration of the sphere centers is known.)

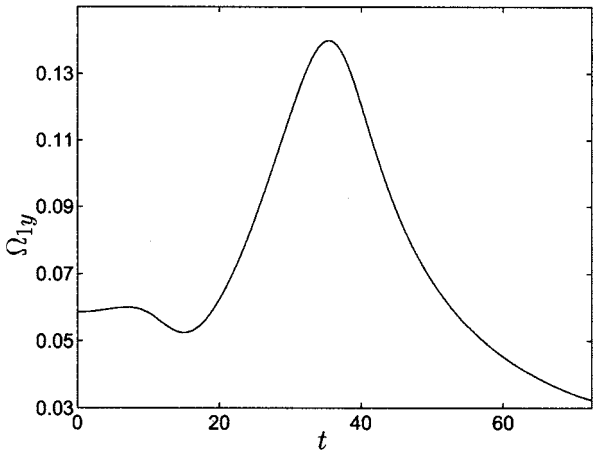


FIG. 8. Angular velocity $\Omega_{1y}(t)$. Initially $x_0=4$, $z_0=0$.

## VI. ASYMPTOTIC SYMMETRICAL DYNAMICS CLOSE TO THE KISSING EQUILIBRIUM

Close to the kissing equilibrium shown in Fig. 3(a), for very small $\xi$ and small $z-z_{\mathrm{eq}}$, it is possible to solve the dynamics (7) and (8) explicitly. To this goal, we express the known external forces and torques exerted on the spheres, $F_{1x}=0$, $F_{1z}=-1$, $\mathcal{T}_{1y}=0$, $F_{2z}=-1$, as linear combinations of the unknown translational and angular velocities $U_{1x}$, $U_{1z}$, $\Omega_{1y}$, $U_{2z}$ of the spheres, with a $4\times 4$ matrix $\boldsymbol{\zeta}$ of the friction coefficients. The simplicity of the friction problem follows from the symmetry of our configuration, since $U_{3x}=-U_{1x}$, $U_{3z}=U_{1z}$, $\Omega_{3y}=-\Omega_{1y}$, and similarly for the forces and the torques. From $\boldsymbol{\zeta}$, we separate out the following two-sphere contribution:

$$\boldsymbol{\zeta}(13)=\begin{pmatrix} X_{11}^A-X_{13}^A & 0 & 0 & 0 \\ 0 & Y_{11}^A+Y_{13}^A & Y_{11}^B+Y_{13}^B & 0 \\ 0 & Y_{11}^B+Y_{13}^B & Y_{11}^C-Y_{13}^C & 0 \\ 0 & 0 & 0 & 0 \end{pmatrix}, \quad (11)$$

with the two-sphere friction matrix components denoted after Ref. [13] by $X_{11}^A$, $X_{13}^A$, $Y_{11}^A$, $Y_{13}^A$, $Y_{11}^B$, $Y_{13}^B$, $Y_{11}^C$, and $Y_{13}^C$. The point is that $X_{11}^A-X_{13}^A$ and $Y_{11}^C-Y_{13}^C$ are the only singular contributions when $\xi\to 0$. We perform the asymptotic expansion of $\boldsymbol{\zeta}$ (13) in $\xi$; we use the Jeffrey-Onishi expressions [13], neglecting terms $O(\xi\ln\xi)$. The rest, $\boldsymbol{\zeta}(123)=\boldsymbol{\zeta}-\boldsymbol{\zeta}(13)$, is a regular function of $\xi$; we evaluate it numerically at the equilibrium. Next, we use MATHEMATICA to invert $\boldsymbol{\zeta}$. Neglecting terms $O(\xi)$, using the relations $\dot{\xi}=2U_{1x}$ and $\dot{z}=U_{1z}-U_{2z}$, and allowing for a small perturbation of $z$ around the equilibrium, we obtain asymptotic approximation of Eqs. (7) and (8),

$$\dot{\xi}=-a\xi, \quad (12)$$

$$\dot{z}=-c(z-z_{\mathrm{eq}})-\frac{e}{\ln\xi^{-1}+b}. \quad (13)$$

The constants $a=0.80$, $b=4.0$, and $e=0.22$ follow from the inversion of $\boldsymbol{\zeta}$ at the equilibrium. The constant $c$ is evaluated numerically as $c=-[\partial v_z(1,z)/\partial z]_{z=z_{\mathrm{eq}}}=0.124$.

By integrating Eq. (12) and the trajectory equation

$$\frac{dz}{d\xi}=\frac{c}{a\xi}(z-z_{\mathrm{eq}})+\frac{e}{a\xi(\ln\xi^{-1}+b)}, \quad (14)$$

the asymptotic solution is easily obtained

$$\xi=\xi_0 e^{-at}, \quad (15)$$

$$z-z_{\mathrm{eq}}=\{(z_0-z_{\mathrm{eq}})e^{\tau_0}-(e/a)[Ei(\tau)-Ei(\tau_0)]\}e^{-\tau}, \quad (16)$$

where $\tau=c(\ln \xi^{-1}+b)/a=c[t+(\ln \xi_0^{-1}+b)/a]$, and its value at $t=0$ is equal to $\tau_0=c(\ln \xi_0^{-1}+b)/a$. As before, $\xi_0=x_0-1$. The symbol $Ei(\tau)$ denotes the exponential integral, the Cauchy principal value of $\int_{-\infty}^{\tau} dte^t/t$.

Precision of the asymptotic solutions (15) and (16) is illustrated in the inset of Fig. 7. For gaps $\xi \lesssim 10^{-4}$, the numerical $z(t)$ is approximated with 5% accuracy by the asymptotic one. Similar estimation holds for $\ln \xi(t)$.

For very large times (for very small gaps $\xi$), $\tau \to \infty$, and $Ei(\tau) \approx (1+1/\tau)e^{\tau}/\tau$. In this case, relation (16) further simplifies,

$$z - z_{\mathrm{eq}} \approx -\frac{e}{c}\frac{1}{\ln \xi^{-1}+b} \quad \text{if } \xi \to 0, \tag{17}$$

and $(x,z) \to (1,z_{\mathrm{eq}})=(1,1.578634)$, if $t \to \infty$. The equilibrium solution $(1,z_{\mathrm{eq}})$ of the dynamics (7) and (8) is stable.

## VII. SYMMETRICAL PHASE PORTRAIT

In Fig. 9, we numerically evaluate the phase portrait for the symmetrical dynamics of spheres (7) and (8). The two-dimensional phase space excludes non-overlapping spheres, and is therefore given as $\{(x,z): x \geqslant 1 \text{ and } x^2/4+z^2 \geqslant 1\}$.

Trajectories of the spheres initially aligned horizontally practically keep the same shape as long as all the spheres are at large distances from each other. As illustrated in Fig. 10, this "ideal" shape is given by the scale-free point-particle dynamics.

In Fig. 9, another family of trajectories is also plotted, with $z=\infty$ at $t=-\infty$. Such pairs of spheres, initially far above the single one, and practically noninteracting with the singlet, decrease the relative vertical distance $z$ with time and tend to the kissing equilibrium, shown in Fig. 3(a); they never reach $z=0$.

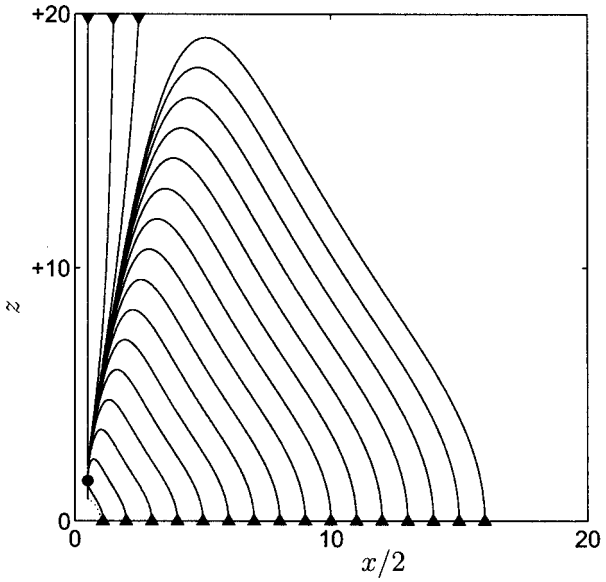


FIG. 9. Phase portrait for the symmetrical dynamics of spheres. The stable "kissing" node (•) is $(x,z)=(1,1.578634)$. Dotted line: unstable "chain" equilibria at $x^2/4+z^2=1$.

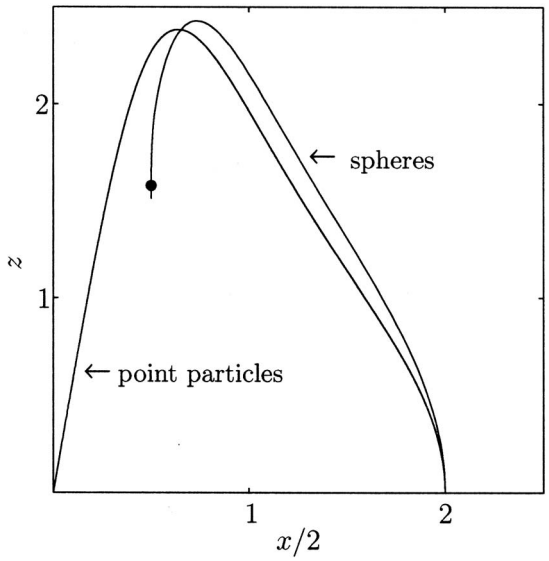


FIG. 10. Sphere trajectory and its point-particle counterpart.

From the last section it follows that the equilibrium $(1,z_{\mathrm{eq}})$ is a stable improper node. At this point, $dz/dx=-\infty$ for all the trajectories. Indeed, according to Eq. (17), $dz/dx \approx -(e/c)/[(\ln \xi^{-1}+b)^2 \xi]$ if $(x,z)$ is sufficiently close to $(1,z_{\mathrm{eq}})$.

To illustrate how the trajectories approach the kissing equilibrium, in Fig. 11 we plot $z$ versus $1/(\ln \xi^{-1}+b)$, using numerical results and asymptotic expressions (16) and (17).

For $z<0$, the motion is obtained by the time reversal superposed with the reflection in the plane $z=0$, using Eq. (10). In particular, the kissing equilibrium $(1,-z_{\mathrm{eq}})$ is an unstable improper node.

It remains to discuss stability of the chain equilibria. To this goal, in Fig. 12 trajectories very close to the chain equilibrium line $x^2/4+z^2=1$ are plotted. They all evolve towards

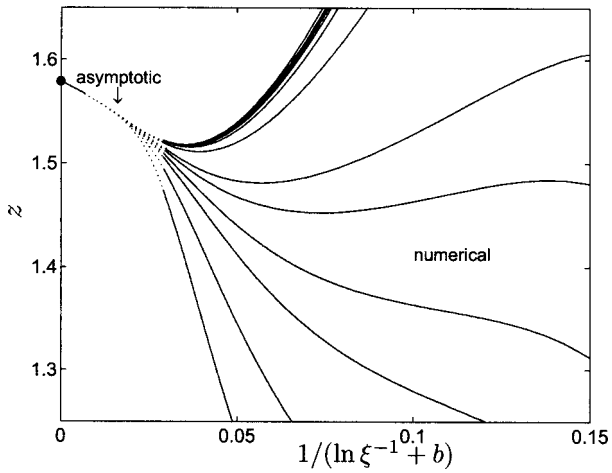


FIG. 11. Phase portrait close to the stable node (•); numerical trajectories as in Fig. 9, plus those with $x_0/2=1.001, 1.01, 1.05, 1.2, 1.3$, and $z_0=0$. For small $\xi$, evolution is continued with the asymptotic expression (16) (dotted line). The limiting straight line (17) is also marked.

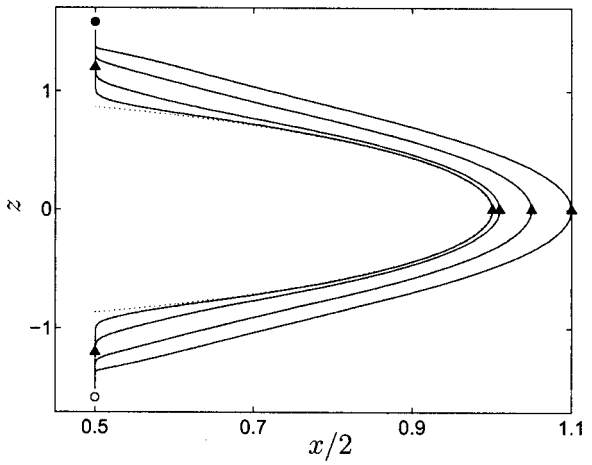


FIG. 12. Numerical trajectories (solid lines) close to the "chain" equilibria (dotted line). Specifically, $x/2=1.001, 1.05, 1.01, 1.1$ at $z=0$.

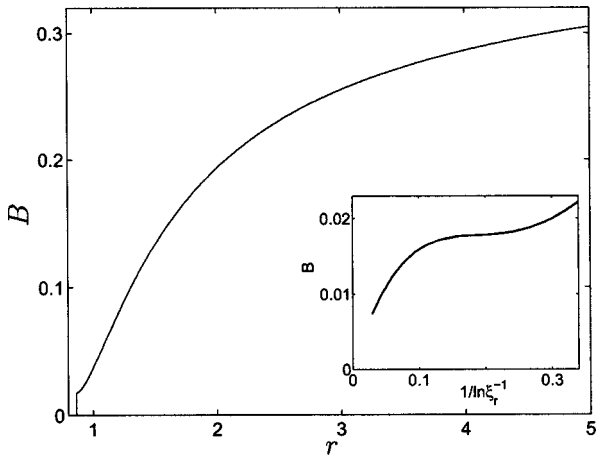


FIG. 14. The mobility function $B(r)$. Inset: for configurations close to equilateral triangles (small $r$), $B$ is plotted versus $1/\ln(r-\sqrt{3}/2)^{-1}$.

the kissing equilibrium [Fig. 3(a)]. These numerical results indicate that the chain equilibria are unstable against the symmetrical perturbations. The symmetrical relative dynamics of spheres has the only stable (kissing) equilibrium at $(x,z)=(1,1.578634)$. In the following, nonsymmetrical configurations will be also considered to check if the symmetrically stable kissing equilibrium is stable against *all* perturbations.

## VIII. ILLUSTRATIVE EXAMPLE OF NONSYMMETRICAL DYNAMICS

A family of initial conditions is considered, with the sphere centers located at vertices of an isosceles triangle with the horizontal base. In general, the triangle is nonvertical. Such a configuration is parametrized by $x$, $y$, and $z$, where $(\boldsymbol{r}_{12}+\boldsymbol{r}_{32})/2=(0,y,z)$ and $\boldsymbol{r}_{31}=(x,0,0)$. Its projection on the $xz$ plane is illustrated in Fig. 1, and projection on the $yz$ plane in Fig. 13. In addition, it is assumed that the base spheres contact with each other $(x=1)$. From symmetry it follows that while such configurations evolve, they retain all these properties.

The dynamics of the relative motion has a simple form in polar coordinates. It is sufficient to consider only $0\leqslant\theta\leqslant\pi$. Owing to symmetry, $F_\theta=F\sin\theta$ gives rise only to the transverse velocity $r\dot{\theta}$, and $F_r=-F\cos\theta$ only to the radial velocity $\dot{r}$. With the chosen normalization $F=1$ and the dynamics reads

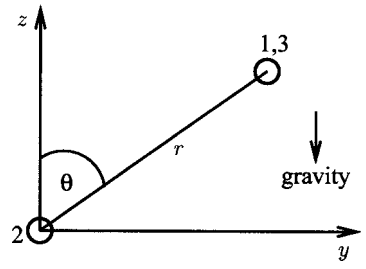


FIG. 13. Configuration at an isosceles triangle with a horizontal base (in general nonvertical). Surfaces of the base spheres touch each other.

$$r\dot{\theta}=B(r)\sin\theta, \tag{18}$$

$$\dot{r}=-C(r)\cos\theta. \tag{19}$$

The mobility function $C(r)=-v_z(1,r)$ has been already calculated and plotted in Fig. 2. The other mobility function $B(r)$ is evaluated in a similar way from the multipole expansion, and plotted in Fig. 14.

Note the importance of transverse lubrication effects. For $\xi_r\equiv r-\sqrt{3}/2\ll 1$ (very small gaps between the surfaces), $B\sim 1/\ln\xi_r^{-1}$. Such a slow decay of the transverse relative translational velocities is related to significant angular velocities of individual spheres. (To compare, radial lubrication effects lead to the linear scaling of the radial relative translational velocities $C\approx-0.7\xi_r$.)

From the dynamics (18) and (19), the phase paths are obtained as

$$\ln\frac{\sin\theta}{\sin\theta_0}=-\int_{r_0}^{r}dr'\frac{B(r')}{r'C(r')},\quad \text{if } r_0\neq z_{\mathrm{eq}}, \tag{20}$$

$$r=z_{\mathrm{eq}},\quad \text{otherwise}, \tag{21}$$

with $r=r_0$ and $\theta=\theta_0$ at $t=0$. The motion along $r=z_{\mathrm{eq}}$ satisfies

$$\frac{\tan\frac{\theta}{2}}{\tan\frac{\theta_0}{2}}=\exp\left[\frac{B(z_{\mathrm{eq}})}{z_{\mathrm{eq}}}t\right], \tag{22}$$

therefore the point $\theta=\pi$ is reached after infinite time. The phase portrait for this dynamics is numerically evaluated and plotted in Fig. 15.

Both kissing equilibria now represent saddle points, and therefore are unstable. There exist a heteroclinic path [16]: a half-circle of radius $r=z_{\mathrm{eq}}\equiv 1.578634$. It separates the regions of closed and open trajectories. If $r\leqslant z_{\mathrm{eq}}$ or $\theta=0$, then the three spheres will for ever stay together within a cluster.

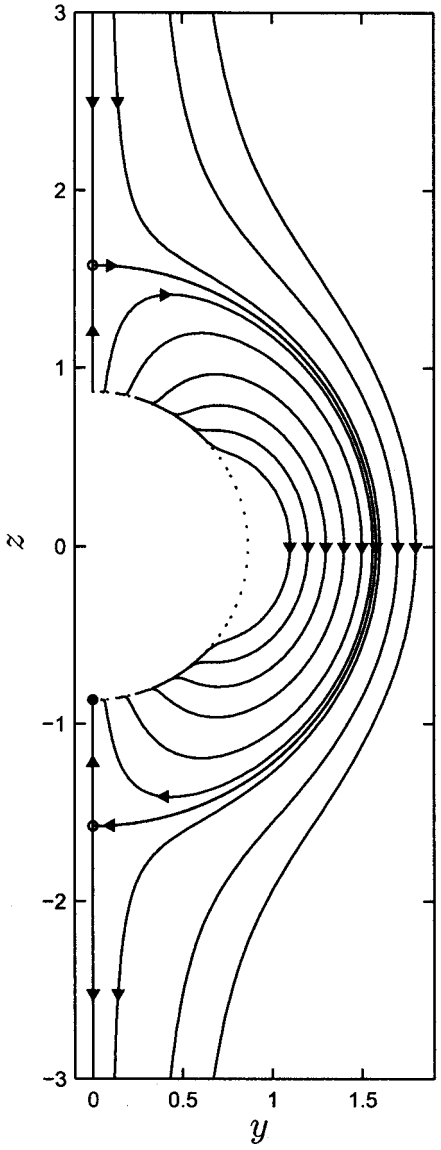


FIG. 15. Phase portrait for the relative dynamics of spheres, which form an isosceles triangle with a horizontal base of unit length. Dotted line: equilibria at equilateral triangles.

The other part of the phase space contains configurations which ultimately split into a faster pair of spheres and a slower singlet.

Additional equilibria for the dynamics (18) and (19) are found at each point of the half-circle $r=\sqrt{3}/2$, by solving $B(r)=C(r)=0$. These equilibria correspond to slanted equilateral triangles. They are also stationary configurations of the general dynamics (2). Each equilibrium with $0\leqslant\theta<\pi$ and $r=\sqrt{3}/2$ is unstable. Indeed, a small perturbation with $\theta'>\theta$ and $r'>\sqrt{3}/2$ is repelled, since $\dot{\theta}'>0$. On the other hand, the equilibrium $\theta=\pi$ and $r=\sqrt{3}/2$ is a stable node—its arbitrary perturbation $(\theta',r')$ is attracted, as it follows from the analysis of signs of $\dot{\theta}'$ and $\dot{r}'$. This ''chain'' configuration, shown in Fig. 3(f), is the only stable equilibrium of the dynamics of isosceles triangles with a horizontal base of unit length.

## IX. CONCLUSIONS

In this work, relative dynamics of three heavy spheres located at vertices of an isosceles vertical triangle with the horizontal base has been investigated. For this symmetrical dynamics, equilibria have been determined and shown in Fig. 3. They contain one, two or three pairs of touching spheres. It has been shown numerically that the equilibria with $y=0$ and $(x,z)=(1,-1.578634)$ or $x^2/4+z^2=1$ [see Figs. 3(b)–3(g)] are unstable against the symmetrical perturbations (5) and (6). For a large class of the initial symmetrical conditions, the system evolves towards the stable node $(x,z)=(1,1.578634)$ [see Fig. 3(a)], reaching it after infinite time. The corresponding point-force solution is singular: after a finite time, all the particles collapse onto a single point with infinite velocities.

A complementary two-dimensional dynamics (in the perpendicular plane) has been also studied: relative motion of configurations with the sphere centers at isosceles (in general nonvertical) triangles with the horizontal base, and the base spheres touching each other. This dynamics contains the symmetrical equilibria at $(x,y,z)=(1,0,\pm z_{\mathrm{eq}})$, $(1,0,\pm\sqrt{3}/2)$, and also a new family of nonsymmetrical equilibria at $x=1$ and $z^2+y^2=3/4$ (slanted equilateral triangles with the spheres at contact). The node $(1,0,-\sqrt{3}/2)$ is the only stable equilibrium of this dynamics. Although both kissing equilibria $(x,y,z)=(1,0,\pm z_{\mathrm{eq}})$ are unstable, they are connected by a separatrix, which discriminates between configurations of spheres, which form a stable cluster, and those which are going to split into two smaller clusters.

The stationary solutions presented here, in addition to their physical and biological importance, may be used as benchmarks for numerical simulations of many-particle systems.

## ACKNOWLEDGMENT

The authors thank Professor Jerzy Bławzdziewicz and Professor Gerhard Nägele for helpful discussions.

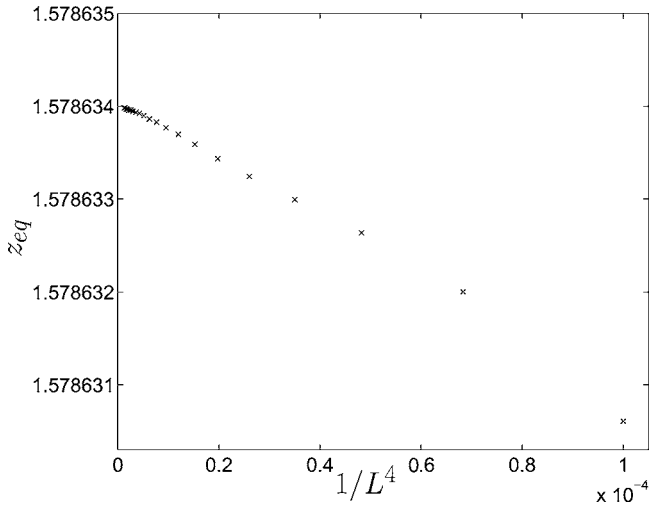


FIG. 16. The equilibrium parameter $z_{\mathrm{eq}}$ versus $1/L^4$.

## APPENDIX: HOW DOES THE KISSING EQUILIBRIUM CONFIGURATION DEPEND ON THE MULTIPOLE ORDER?

In this Appendix, the equilibrium separation $z_{eq}$ between the kissing pair and the singlet is calculated for all the multipole orders $1 \leqslant L \leqslant 30$. For $L \geqslant 10$, the results are depicted in Fig. 16, and for $L \leqslant 10$, in Table I.

As illustrated in Fig. 16, in the limit $L \to \infty$ one recovers Eq. (9) with $z_{eq}=1.578634$. Note that, according to Table I, the kissing equilibrium configuration is determined with 2% accuracy even if the multipole expansion is truncated at as low multipole order as $L=1$. The multipole order $L=4$, used in this paper to evaluate evolution, is standard for precise calculations [11]. Here, it gives $z_{eq}$ with the $10^{-4}$ accuracy.

TABLE I. The equilibrium parameter $z_{eq}$ for low values of $L$.

| $L$ | $z_{eq}$ |
|---|---|
| 1 | 1.544187 |
| 2 | 1.577183 |
| 3 | 1.579872 |
| 4 | 1.578783 |
| 5 | 1.578620 |
| 6 | 1.578610 |
| 7 | 1.578613 |
| 8 | 1.578621 |
| 9 | 1.578627 |
| 10 | 1.578631 |


[1] H. C. Berg, Phys. Today **53**, 24 (2000).
[2] I. M. Jánosi, T. Tél, D. E. Wolf, and J. A. C. Gallas, Phys. Rev. E **56**, 2858 (1997).
[3] L. M. Hocking, J. Fluid Mech. **20**, 129 (1964).
[4] R. E. Caflisch, C. Lim, J. H. C. Luke, and A. S. Sangani, Phys. Fluids **31**, 3175 (1988).
[5] C. C. Lim and I. H. McComb, J. Diff. Eqns. **121**, 384 (1995).
[6] M. L. Ekiel-Jeżewska and E. Wajnryb, Arch. Mech. (to be published).
[7] J. Happel and H. Brenner, *Low Reynolds Number Hydrodynamics* (Kluwer Academic Publishers, Leyden, 1991).
[8] S. Kim and S. J. Karrila, *Microhydrodynamics* (Butterworth-Heinemann, Boston, 1991).
[9] B. U. Felderhof, Physica A **151**, 1 (1988).
[10] B. Cichocki, B. U. Felderhof, K. Hinsen, E. Wajnryb, and J. Bławzdziewicz, J. Chem. Phys. **100**, 3780 (1994).
[11] B. Cichocki, M. L. Ekiel-Jeżewska, and E. Wajnryb, J. Chem. Phys. **111**, 3265 (1999).
[12] W. H. Press, S. A. Teukolsky, W. T. Vetterling, and B. P. Flannery, *Numerical Recipes* (Cambridge University Press, Cambridge, 1992).
[13] D. J. Jeffrey and Y. Onishi, J. Fluid Mech. **139**, 261 (1984).
[14] B. Cichocki, M. L. Ekiel-Jeżewska, G. Nägele, and E. Wajnryb, J. Chem. Phys. **121**, 2305 (2004).
[15] See EPAPS Document No. E-PLEEE8-73-187603 for a movie illustrating the difference between evolution of three point forces and three heavy spheres, initially aligned horizontally. The particles settle in a viscous fluid under identical vertical gravitational forces. Their relative motion is shown in the frame of reference moving with the middle (red) particle. This document can be reached via a direct link in the online article's HTML reference section or via the EPAPS homepage (http://www.aip.org/pubservs/epaps.html). Also http://www.ippt.gov.pl/~mekiel
[16] D. W. Jordan and P. Smith, *Nonlinear Ordinary Differential Equations* (Clarendon, Oxford, 1987).